Understanding the Shape Memory Behavior of Self-Bending Materials and Their Use as Sensors

Xue Li, Michael J. Serpe*

Department of Chemistry, University of Alberta, Edmonton, AB T6G 2G2, Canada

*Corresponding Author -- michael.serpe@ualberta.ca

Keywords: Stimuli responsive polymers, Shape memory materials, Humidity responsive actuators, Humidity sensing, Stretchable conductors

Abstract

By depositing layers composed of poly (N-isopropylacrylamide) (pNIPAm)-based microgels and the polyelectrolyte polydiallyldimethylammonium chloride (pDADMAC) on a flexible substrate, responsive materials that bend upon drying could be fabricated — the extent of the bending depended on atmospheric humidity. Here, we show that the bending conformation/direction could be templated, and exhibits shape memory. We examined in detail the bilayer system, which led to an understanding of the phenomena leading to this behavior. By close examination of microscopy images and diffraction patterns, we were able to determine that the dried polymer-based layer was composed of both amorphous and crystalline phases — the amorphous phase can readily absorb water, which results in actuation, while the crystalline phases template the bending characteristics of the device. With an understanding of the bending behavior of the devices, we were able to generate humidity sensors by interfacing them with stretchable strain sensors, which were also developed here specifically for the bendable materials here.

Introduction

Actuators composed of responsive (i.e., smart or stimuli responsive) polymers/materials are capable of reversibly changing their shape, size, and/or mechanical properties in response to external stimuli. Actuators have found applications as/in sensors,[1-3] artificial muscles,[4, 5] controlled encapsulation/delivery vehicles,[6] biomimetic actuating systems,[7] and soft robotics.[8] Generally, the bending and unbending motions of polymer-based actuators relies on the inhomogeneous asymmetric contraction or expansion in a material.[9] A variety of stimuli responsive polymers and materials, such as liquid crystalline polymers, hydrogels, shape memory polymers (SMP), and elastomers have been fabricated to make sensors and actuators.[10-13] Of the stimuli responsive polymers, poly (N-isopropylacrylamide) (pNIPAm) is the most extensively studied. PNIPAm is well known to exhibit a lower critical solution temperature (LCST) and the polymer collapses/deswells in water above 32 °C. The transition is fully reversible, i.e., when the water temperature is reduced to below 32 °C the polymer expands/reswells. The deswelling/reswelling process can be repeated over many cycles without a loss in responsivity.[14] PNIPAm-based networks can also be synthesized, and exhibit swelling/deswelling behavior similar to linear pNIPAm, i.e., the hydrogel network deswells and swells at high and low temperature, respectively. Colloidally stable hydrogel micro and nanoparticles (microgels and nanogels, respectively) can be synthesized and also exhibit the same temperature responsivity. PNIPAm-based materials can be made responsive to other stimuli by copolymerization of other functional monomers into the system.[15, 16] One common example is to incorporate acrylic acid (AAc) (with a pKa of ~4.25) into pNIPAm-based microgels to form pH responsive microgels. That is, at high pH values, the

microgels swell due to the generation of charges in the microgel network (due to AAc deprotonation) and the resulting charge-charge repulsion and osmotic swelling.[17]

So called "shape memory polymers" (SMP) are another interesting class of stimuli responsive materials that have been used for actuation.[18] A conventional SMP exists in some initial (or permanent) shape, which can be changed when exposed to specific environmental conditions (typically high temperature). With the material trapped (typically physically) in the temporary state, the environmental conditions can be returned back to their initial state, which traps the material in its temporary state. The SMP can return to its permanent shape once the environmental conditions return to the state where the temporary state was formed.[19-21] Recent results have shown that shape memory materials can be achieved without the use of standard SMPs. For example, Ionov and coworkers reported on a polymer-based actuator composed of biodegradable polycaprolactone (PCL)-gelatin bilayers, which are unfolded at room temperature and folded at temperature above PCL's T_m.[22] This is because PCL is crystalline and stiff at low temperature, which prevents any shape change of the material. Heating the PCL above its T_m allows the material to deform due to the melting of the polymer. Cooling down leads to the recrystallization of the PCL and induces the polymer film to recover its unfolded shape.

In previous studies, we showed that polymer-based actuators could be fabricated by depositing a layer of polydiallyldimethylammonium chloride (pDADMAC) on a single layer of pNIPAm - based microgels attached to a Au-coated semi-rigid plastic substrate. These materials are able to act as actuators/muscles in response to humidity.[5] They are able to lift large masses, and resist forces, many times their own mass. We also investigated how the size and aspect ratio of the polymer substrate affected the self-bending behavior of the materials. From experimental observations, a set of empirical rules were developed that could be used to predict the self-bending behavior. From these rules, we were

able to direct the bending of these materials into discrete three-dimensional objects, which are fully capable of unbending and bending in response to humidity.[23]

Strain sensors, with high flexibilities and stretchability, have the ability to transduce physical forces (including bending and twisting) and chemical stimuli into electrical signals.[24-27] These devices play a key role in many emerging technologies, such as: intelligent robotic sensing systems,[28] human motion and health monitoring,[29, 30] and electronic skin.[31, 32] One typical approach to fabricating strain sensors is to impregnate flexible/stretchable polymer materials with conductive species. Nanoscale fillers (e.g., carbon nanotubes, graphene, metal nanowires, and metal nanoparticles) incorporated into flexible polymers have been shown to be effective for producing these devices. Several reviews have been published that illustrate how conductive nanostructures can be used for strain sensing applications.[26, 33-35] However, in many cases they exhibit high electrical resistivity that may change significantly under strain and the conductivity is typically too low to be useful, leading to poor performance and reliability.[36] One alternative is to deposit thin films of highly conductive metal or alloy onto elastomeric substrates and those metal films on elastomeric substrates are sensitive to strain by fracturing or buckling, while retaining relatively high conductivity.[37]

In this study, we first report on a shape memory material fabricated by deposition of pNIPAm-co-AAc microgel and polyelectrolyte layers on a plastic substrate, to generate a bilayer structure. We show that these bilayers have the ability to change shape/bend in response to environmental humidity. Importantly, the bilayer devices investigated here exhibit bending behavior that is unique compared to devices that we previously characterized.[5,22] That is, their self-bending behavior is not capable of being predicted using our previously developed models,[23] and appear to be a result of "templated" self bending orientations, which are a result of a shape memory like effect. We hypothesize that the effect comes from the formation of semicrystalline domains in the pDADMAC layer on drying. To the best of

our knowledge, this is the first time the shape memory effect have been observed and studied for pDADMAC-based actuators. We not only fully characterized these materials and the "templated" bending directions, but we also used this behavior to design novel and fully reusable humidity responsive sensors and actuators. While we show the device's utility for sensing humidity, the structure can be easily modified to detect other variables/species of interest.

Results and discussion

Shape memory effect study of bilayer systems

A schematic of the devices used in this investigation is shown in Figure 1. Specifically, onto circular plastic substrates (5.5 cm diameter) 2 nm Cr and 50 nm Au were deposited via thermal evaporation followed by painting pNIPAm-co-AAc microgels onto the resulting substrate, and finally a solution containing positively charged pDADMAC (20 wt % in water) was added onto the microgels and allowed to dry.[5] Importantly, the pDADMAC solution has a pH of ~6.5, which renders the pDADMAC positively charged, while the AAc in the microgels is deprotonated and hence negatively charged. The many electrostatic interactions between these species allows the pDADMAC layer to strongly adhere to the microgel layer. Furthermore, since the microgel layer is strongly adhered to the Au-coated flexible substrate, the contraction of the pDADMAC layer upon drying is translated into bending of the flexible substrate. We consider the resulting devices as bilayers — the top layer being composed of pDADMAC and microgels and the bottom layer is the Au and plastic. Upon drying the pDADMAC layer at 5% relative humidity, the device bends along one central axis and the resultant shape and degree of bending depends on the size/shape of the flexible substrate, and the amount of pDADMAC deposited on the microgel coated flexible substrates.[5, 22] It is also important to note that pDADMAC itself doesn't bend significantly upon drying, and the fact that it is strongly bound to the flexible substrate allows the contraction upon drying to be translated into device bending. The device

subsequently opens (unbends) when it is exposed to an environment with a relative humidity of 55%; this is due to the pDADMAC layer absorbing water from the environment, hydrating, and expanding. The bending and unbending process can be repeated many times and each time the device bends along the central axis that was formed during the initial bending. Thus the devices exhibit shape changing behavior and *shape memory* since the bent and unbent conformations are reproducible over many cycles.

Figure 2a shows a photograph of a typical bent circular device that was fabricated as part of this investigation. For this investigation, three devices were fabricated in the same way, with the same dimensions and each showed the same bending behavior as the device shown in Figure 2a. When each of the three devices was opened, rectangular portions (0.8 cm × 3 cm) were cut out of each device, with different orientations relative to the bending axis; this is shown in Figure 2b-d — these are referred to as templated devices. As can be seen in Figure 2e, each of the rectangular portions bend into a specific conformation defined by where they were cut from the circular device, and the cutting orientation/direction relative to the bending axis. In other words, they bend into a conformation that exactly matches how they would have bent if they were still part of the circular device they were cut from. For comparison, three separate rectangular devices (untemplated devices) with the same dimensions of those in Figure 2e (0.8 cm × 3cm) were fabricated in the same way as the circular devices, although the devices were not prebent prior to their generation. The rectangular devices were allowed to bend under the same conditions as the devices in Fig 2e, and as can be seen in Figure 2f, the devices bend in a completely different manner relative to those devices cut from the circular "parent" devices. In fact, the bending behavior of the devices in Figure 2f can be predicted from our previously developed models, while our current models could not explain the bending behavior of the devices in Figure 2e. We also point out that all the respective devices bend in the same way over many bending/unbending cycles, suggesting that the bending direction is permanently templated into the devices.

To explain the bending of the untemplated devices in Figure 2f, we consider some recently published examples of self-bending bilayers.[38-41] Many bilayers constructed from inorganic and polymer-based materials exhibit self-bending behavior due to the relaxation of internal stresses that originate from dissimilar properties of the two layers, e.g., lattice mismatches, thermal expansion coefficients, and swelling abilities. The size and shape of the bilayers also have a significant effect on the bending behavior that can yield "long-side", "short-side" and "diagonal" bending.[42-44] In other words, the way devices bend depends on the dimensions of the devices, and their specific aspect ratios. Thus, the bending behavior of the untemplated devices is directly related to their shape, size, and aspect ratio; the devices will bend in the direction (and into a shape) that minimizes resistance to bending. In the case of the untemplated devices here, long-side bending is the preferred bending direction, as can be seen in Figure 2f. On the other hand, the templated devices show completely different bending behavior, allowing them to bend in ways that are not preferred (Figure 2e), and into configurations that require bending in directions/conformations of high resistance. In order to explain this behavior, we defined the shape of the circular device after bending in low humidity as the "permanent shape" (also called "memorized shape"). Since the circular device is symmetric, it always bends into a tube configuration, which yields the minimum resistance to bending. By exposing the devices to high humidity, they can be fixed into unbent "temporary states". They have the ability to bend back to the permanent shape when the humidity is again decreased. Therefore, any portion of the circular device will be templated to bend in the direction that was originally dictated by the "parent" circular device, thus allowing the materials to reproducibly change shape with changes in humidity. This reproducible bending behavior can be considered to impart shape memory to our materials, although it is for different reasons than what is seen in typical shape memory polymers.

To explain the shape memory function of our devices (and the templating effect), we investigated the properties of the pDADMAC layer via X-ray diffraction (XRD) analysis. XRD was performed on a pDADMAC film deposited on (100) silicon substrate, and the obtained XRD pattern is shown in Figure 3a. We have assigned the broad and strong peaks at 2θ at 16.19°, 21.80°, and 34.05° to the polymer itself, showing both crystalline and amorphous phases. The rest of the diffraction peaks could be attributed to sodium chloride (NaCl), which exist in the polymer solution. Furthermore, we investigated whether crystalline phases can be observed throughout the thickness of the polyelectrolyte layer. To investigate this, we microtomed the pDADMAC layer into thin polymer slices, each with a thickness of 100 nm and analyzed the film structure by transmission electron microscopy (TEM). From the TEM images in Figure 3b, it can be seen that there are two distinct regions — a grey bulk region and small dark clusters dispersed in the film. Electron diffraction analysis was performed on these two regions, and as can be seen in Figure 3c, the diffraction pattern for the dark clusters was proven to be NaCl while the diffraction pattern for the grey bulk region shows weaker (although present) features, as can be seen in Figure 3d. These further prove the semicrystallization of the polyelectrolyte layer. The TEM image (Figure 3e) of the grey bulk film in large magnification reveals that there are density differences on the polymer film, which is indicative of two distinct regions in the layer. This could be a proof that the film contains both crystalline and amorphous phases.

Based on above results, we propose the observed shape memory bending/unbending behavior of our templated devices is a result of the formation of both crystallized and amorphous phases in the pDADMAC layer. Specifically, upon deposition of the pDADMAC solution onto the microgel layer, the chains are in a fully extended state, as a result of the highly charged monomer units in the polymer backbone repelling each other via electrostatic repulsion, and resultant electrostatic double layer-like effects. At low humidity, the pDADMAC solution dries, and the concentration of both the pDADMAC

and the counterions in solution increases. The increase in counterion concentration increases the screening effect of pDADMAC's charged units — this allows the polymer chains to contract, and get closer to one another. Under these conditions, strong intermolecular interactions and entanglements between polymer chains can result in the formation of both crystalline and amorphous phases in the pDADMAC layer. We point out that NaCl crystals can serve as nucleation sites for pDADMAC crystallization, but this is not required for crystalline phase formation. In fact, Lu and coworkers have shown that crystallization could be observed in pure pDADMAC thin films.[45]

While the discussion above details how crystalline phases are formed, it still does not account for the observed shape memory. To explain this, we show a schematic of a bent device in Figure 4a. As can be seen, the device bends along one central axis into a tubular structure. As a result of drying, the device bends and crystalline phases are formed throughout the pDADMAC layer (described above), separated by amorphous phases; the crystalline phases are *hypothesized* to align perpendicular to the bending axis. We propose that it is the alignment of the crystalline phases with the bending axis that locks the bending direction of the devices in place. When exposing the bent device to high humidity, the amorphous phases swell more readily than the crystalline phases, leading to unbending of the device. This is shown schematically in Figure 4b. It is important to note that the crystalline phases retain their structure at high humidity, while the amorphous phases become soft and swollen — it is the retention of the crystalline phases that templates the shape memory. This concept is supported by previous studies that show that water may serve as a plasticizer of pDADMAC, which decreases its glass transition temperature (Tg), which is 70 $^{\circ}$C for pDADMAC.[46] Therefore, as water is sorbed, the amorphous phases become soft and swollen, allowing the device to unbend. At the humidity required for unbending, the crystalline phases remain intact, which is also supported by literature precedent.[47, 48] Finally, any portion cut from the prebent circular device will likewise retain these crystalline structures and orientations, which allows

them bend/unbend in the same manner each time. Therefore, the individual portions cut from the prebent circular device will bend as it would if it were never cut from the circular "parent" device, exhibiting a shape memory-like effect. We point out again that pDADMAC itself is not a shape memory polymer, although our bilayer devices allow it to bend flexible substrates into specific shapes, and these devices exhibit shape memory. This concept is illustrated schematically in Figure 5. As can be seen schematically in Figure 5a, when the rectangle is cut perpendicular to the bending axis, the device bends along the long axis, while it bends on the short axis if the rectangle is cut parallel to the original bending axis, as shown schematically in Figure 5b. Similar arguments can be made for any other devices (rectangular or otherwise) cut from different parts of the original circular device, and with any orientation relative to the bending axis.

It is worth noting that the mechanism of shape memory that we describe here is much different than for common temperature triggered shape memory polymers, which relies on increasing and decreasing their temperature above and below the material's melting or glass transition temperature to yield material deformation. To the best of our knowledge, this is the first time that the crystallization of polyelectrolytes has been used to explain the shape memory behavior and deformation of devices.

Applications

With the shape memory behavior of our systems described, we used these devices to construct novel humidity sensors. Specifically, we cut rectangular pieces from a circular device (as above) and coupled them to strain sensors that are capable of changing their electrical properties (resistance/conductivity changes) upon stretching and/or bending. We also used these sensors as an electrical component in a circuit that was coupled to a light emitting diode (LED). This allowed the resistance changes of the strain sensors to modulate the intensity of the light emitted from the LED.

First, we fabricated the strain sensor as shown schematically in Figure 6a. A 0.5 mm thick polydimethylsiloxane (PDMS) film was generated by mixing commercially available silicone elastomer base gel and curing agent in a 10:1 volume ratio and curing overnight at 70 $^{\circ}$C on a plastic substrate. A thermal evaporator was then used to deposit 2 nm of Cr followed by 50 nm Au onto the PDMS. The resultant material was then cut into 10 mm wide x 25 mm long pieces. Figure 6b shows the field emission scanning electron microscope (FESEM) image of the surface of the hybrid material, which revealed connected Au "islands" with an average grain size of ~13 nm. Figure 6c shows the X-ray photoelectron spectroscopy (XPS) analysis of the surface, which reveals characteristic signals for Au, O and Si. Finally, we show that the devices are bendable and stretchable, as shown in Figure 6d and 6e.

Figure 7a shows schematically how the resultant device was used as a strain sensor. Both ends of the device were clipped to electrical connectors, and a multimeter was used to determine the resistance of the devices as a function of applied strain, i.e., length increase compared to original length. Specifically, we determined the resistance as a function of stretching degree for strains of 0, 5, 10, 15, 20, 25, and 30 % — the resistance was recorded for both stretching and unstretching. The stretching/unstretching was repeated three times and the results are shown in Figure 7b. Furthermore, we introduced this device as a component of an electrical circuit composed of a LED and a battery and showed that the light intensity could be modulated by stretching/unstretching the hybrid material in the same manner as above. The intensity of the LED light at the different strains is shown in Figure 7b. As can be seen, there is some hysteresis between multiple stretching and unstretching cycles, although the distinct strains can be measured.

We point out that the mechanical properties and conductive behavior of PDMS coated with Au was reported previously, although no systematically study exists on the reversibility and precision of the response over many stretching cycles.[37, 49, 50] Here we further examined the morphology of the gold

surface of the Au-coated PDMS using atomic force microscopy (AFM) and FESEM to understand why the electrical properties of the hybrid depended on the strain. Figure 8a shows schematically how the Au structure changes with strain, while Figures 8b and c are the corresponding AFM and FESEM images of the strained device. Before stretching the "as-deposited" Au layers appeared to be flat, consisting of islands with nanoscale dimensions. When the device was imaged while being held in a stretched state (15% strain), small lateral and transversal microcracks appear in the Au layer, which explained the increase in electrical resistance upon stretching the device. When the strain was increased near 30%, the crack number increased, with a concomitant increase in crack width. The combination of the increase in lateral and transversal cracks directly leads to the increased electrical resistance. When the strain is reduced, the Au film nearly flattens out, and the cracks disappear, leading to the decrease in resistance. This behavior explains the reversibility of the electrical properties of the hybrid during the strain cycles.

Finally, we attached the bendable bilayer devices to the strain sensors to yield a humidity sensor. Specifically, strong van der Waals forces were used to adhere the uncoated side of a *templated* bilayer device to the uncoated side of the Au-coated PDMS. Therefore, the bending/unbending behavior of the bilayer piece will likewise cause the strain sensor to bend resulting in stretching/unstretching (Au film cracking/uncracking), and electrical resistance changes. The templated devices were chosen for these experiments as they exhibited more reproducible and predictable bending behavior relative to the untemplated devices. To investigate the humidity response, we connected the assembly to a multimeter (attached onto the gold surface of the strain sensor) and put the setup in a humidity-controlled chamber. As can be seen in the data in Figure 9b, at a humidity of 45%, the assembly was flat. In this condition, the resistance of the strain sensor was relatively small. When the humidity was decreased to 35%, the device bent, resulting in an increased resistance. We subsequently lowered the humidity to 5% in 10% increments and measured the resistance. As can be seen in Figure 9b, the resistance decreased in a linear

fashion with decreasing humidity. When the humidity was increased from 5% to 45% (in 10% increments), the resistance increased in a linear fashion, and closely followed the resistance for the decrease cycle with little hysteresis. Also, we connected the assembly to a circuit composed of a LED and battery and collected the LED light intensity as a function of humidity — this is shown schematically in Figure 9a. As can be seen in Figure 9b, the light intensity likewise depended on humidity. That is, as the humidity decreased the LED light intensity increased (due to the decreased resistance), while the LED light intensity decreased as the humidity increased (due to the increase in resistance). There was nearly no hysteresis between multiple humidity increase and decrease cycles. This proves that our bilayer self-bending devices can be used as humidity sensors, and could be further developed into sensors for other vapors.

Conclusions

In this work we fully characterized the self-bending behavior of humidity responsive polymer-based bilayer devices. We showed that the bending behavior was greatly influenced by the bending history of the materials they were taken from. Specifically, if rectangular bilayer devices were cut from prebent circular devices, they bent in a manner that directly matched the bending behavior of the region they were taken from. From this behavior we proposed that the pDADMAC layer forms both amorphous and crystalline phases — the crystalline phases template in the bending behavior, which is supported by experimental data. Finally, we fabricated strain sensors that could be coupled to the self-bending materials to yield humidity sensors. While these devices can be used as vapor sensors, they could find utility as soft robotics, and as biomedical devices.

Experimental

Materials: N-isopropylacrylamide (NIPAm) was purchased from TCI (Portland, Oregon) and purified by recrystallization from hexanes (ACS reagent grade, EMD, Gibbstown, NJ) prior to use. N, N'-methylenebisacrylamide (BIS) (99%), acrylic acid (AAc) (99%), and ammonium persulfate (APS) (98+ %) were obtained from Sigma-Aldrich (Oakville, Ontario) and were used as received. Poly (diallyldimethylammonium chloride) solution (pDADMAC) with a MW 100,000 ~ 200,000 (20wt % in water) was purchased from Sigma-Aldrich (St. Louis, MO). Sylgard 184 silicone elastomer base and Sylgard 184 silicone elastomer curing agent were purchased from Dow Corning Corporation, Midland, MI, USA. Deionized (DI) water with a resistivity of 18.2 MΩ•cm was used. Cr/Au annealing was done in a Thermolyne muffle furnace from Thermo Fisher Scientific (Ottawa, Ontario). Anhydrous ethanol was obtained from Commercial Alcohols (Brampton, Ontario). Cr was 99.999% and obtained from ESPI (Ashland, OR), while Au was 99.99% and obtained from MRCS Canada (Edmonton, AB).

Microgel Synthesis: Microgels composed of poly (N-isopropylacrylamide)-co-acrylic acid (pNIPAm-co-AAc) were synthesized via free-radical precipitation polymerization as described previously.[51] The monomer mixture, with a total concentration of 154 mM, was comprised of 85% (mole/mole) NIPAm, 10% AAc, and 5% BIS as the crosslinker. NIPAm (17.0 mmol), and BIS (1.0 mmol) were dissolved in deionized water (100 mL) with stirring in a beaker. The mixture was filtered through a 0.2 μm filter affixed to a 20 mL syringe into a 200 mL 3-necked round-bottom flask. The beaker was rinsed with 25 mL of deionized water and then filtered into the NIPAm/BIS

solution. The flask was then equipped with a temperature probe, a condenser and a N_2 gas inlet. The solution was bubbled with N_2 gas for ~1.5 h, while stirring at a rate of 450 rpm, allowing the temperature to reach 45 °C. AAc (2.0 mmol) was then added to the heated mixture with a micropipette in one aliquot. An aqueous solution of APS (0.078 M, 5 mL) was delivered to the reaction flask with a transfer pipet to initiate the reaction. Immediately following initiation, a temperature ramp of 45 to 65 °C was applied to the solution at a rate of 30 °C/h. The reaction was allowed to proceed overnight at 65 °C. After polymerization, the reaction mixture was allowed to cool down to room temperature and filtered through glass wool to remove any large aggregates. The coagulum was rinsed with deionized water and filtered. Aliquots of these microgels (12 mL) were centrifuged at a speed of ~8500 relative centrifugal force (rcf) at 23 °C for ~ 40 minutes to produce a pellet at the bottom of the centrifuge tube. The supernatant was removed from the pellet of microgels, which was then resuspended to the original volume (12 mL) using deionized water. This process was repeated until the microgels were cleaned.

Fabrication of Self-Bending Bilayers: Transparent flexible plastic sheets (transparency films for high temperature laser copiers from 3M company, Canada) were rinsed with DI water and ethanol and dried with N_2 gas, and 2 nm of Cr followed by 50 nm of Au were thermally evaporated onto them at a rate of ~0.2 Å s-1 and ~0.1 Å s-1, respectively, using a Torr International Inc. model THEUPG thermal evaporation system (New Windsor, NY). The Cr acts as adhesion layer to hold the Au layer on the plastic. An aliquot of about 12 mL of previously purified microgel solution was centrifuged for 30 min at 23 °C at ~8500 relative centrifugal force (rcf) to pack the microgels into a pellet at the bottom of the tube. After removal of the supernatant solution, the microgel pellet was vortexed and placed onto a hot plate at 30 °C. A previously coated Cr/Au substrate was rinsed with ethanol, dried with N_2, and then placed onto a hot plate (Corning, NY) set to 30 °C. Aliquots (40 µL

for each 25 × 25 mm area) of the concentrated microgels were put onto the substrate and then spread toward each edge using the side of a micropipette tip, as previously described. The microgel solution was allowed to dry completely on the substrate for 2 h with the hot plate temperature set to 35°C. Then the substrates were washed copiously with DI water to remove any excess microgels not bound directly to the Au. The microgel painted substrates were then soaked in DI water bath and allowed to incubate overnight on a hot plate set to ~30 °C. Following this step, the substrate was again rinsed with DI water to further remove any microgels not bound directly to the Au coated substrate surface. The microgel painted Au coated substrate was dried with N_2 gas and a specific amount of pDADMAC solution (pH 6.5, 20 wt% in water) was deposited onto the microgel layer. The whole set up was undisturbed and dried at ambient temperature/humidity. After complete drying of the pDADMAC layer, the devices were placed into a humidity controlled chamber. The humidity was controlled with an electronic feedback mechanism to maintain a steady humidity -- humidity was modulated using a Air-O-Swiss AOS 7145 Cool Mist Ultrasonic humidifier (manufactured by Swiss Pure Air).

Fabrication of Au-PDMS Hybrid Strain Sensors: A PDMS film with a thickness of 0.5 mm was made by mixing silicone elastomer base and curing agent (from Dow Corning) in volume ratio of 10:1. Then the resulting film was rinsed with DI water and ethanol and dried with N_2 gas, and 2 nm of Cr followed by 50 nm of Au were thermally evaporated onto the PDMS at a rate of ~0.2 Å s-1 and ~0.1 Å s-1, respectively, using a Torr International Inc. model THEUPG thermal evaporation system. The sensor devices were evaluated by measuring their resistance using a multimeter. To evaluate the sensor resistance as a function of stretching, the electrodes of a multimeter were continuously in contact with the two ends of the device. To evaluate the sensor resistance as a function of bending (when coupled to the self-bending devices), one end of the sensor was clamped,

and attached to the multimeter electrode, while the other electrode was only attached to the sensor device after it completed bending at a given humidity. Additionally, the sensor devices were incorporated in a circuit composed of a battery and a green LED (~532 nm emission center) — the resistance of the sensor device could control the intensity of the LED. Similar to the above approach, the LED was continuously connected to the sensor device for the stretching experiments, while the LED was only connected to the sensor devices after complete bending. We quantified the intensity of the LED using a fiber optic probe to collect the light, which was coupled to a USB2000+ spectrophotometer all from Ocean Optics (Dunedin, FL).

X-ray Diffraction: A polymer film sample was prepared by dropping 0.5 mL pDADMAC solution on a silicon (100) substrate. Then we placed it in a humidity chamber held at 5% humidity until the layer dried. A Rigaku XRD Ultima IV using CuKα X-ray source (40 kV, 44 mA) and continuous scan mode was used to collect data, which was examined using JADE software.

Transmission Electron Microscopy and Electron Diffraction: The dried pDADMAC layer was first microtomed into thin films with a thickness of 100 nm by a LEICA EM UC6 and the thin films were floated onto acetone. Then the thin films were placed on carbon-coated, copper grids. Within a short time, the acetone evaporated and the thin films were well attached onto the grids. Then TEM images and electron diffraction on specific areas were obtained by CM20FEG/STEM, operated at 200 kV.

References

[1] R. Bashir, J.Z. Hilt, O. Elibol, A. Gupta, N.A. Peppas, *Appl. Phys. Lett.* **2002**, 81, 3091-3093.
[2] S. Singamaneni, M.E. McConney, M.C. LeMieux, H. Jiang, J.O. Enlow, T.J. Bunning, R.R. Naik, V.V. Tsukruk, *Adv. Mater.* **2007**, 19, 4248-4255.
[3] K.D. Harris, C.W.M. Bastiaansen, J. Lub, D.J. Broer, *Nano Lett.* **2005**, 5, 1857-1860.
[4] M. Yamada, M. Kondo, J.-i. Mamiya, Y. Yu, M. Kinoshita, C.J. Barrett, T. Ikeda, *Angew. Chem. Int. Ed.* **2008**, 47, 4986-4988.
[5] M.R. Islam, X. Li, K. Smyth, M.J. Serpe, *Angew. Chem. Int. Ed.* **2013**, 125, 10520-10523.
[6] R. Fernandes, D.H. Gracias, *Adv. Drug Deliv. Rev.* **2012**, 64, 1579-1589.
[7] L. Ionov, *Adv. Funct. Mater.* **2013**, 23, 4555-4570.
[8] F. Ilievski, A.D. Mazzeo, R.F. Shepherd, X. Chen, G.M. Whitesides, *Angew. Chem. Int. Ed.* **2011**, 50, 1890-1895.
[9] Y. Osada, *Adv. Mater.* **1993**, 5, 313-314.
[10] C. Ohm, M. Brehmer, R. Zentel, *Adv. Mater.* **2010**, 22, 3366-3387.
[11] Z. Hu, X. Zhang, Y. Li, *Science* **1995**, 269, 525-527.
[12] D.L. Thomsen, P. Keller, J. Naciri, R. Pink, H. Jeon, D. Shenoy, B.R. Ratna, *Macromolecules* **2001**, 34, 5868-5875.
[13] M. Behl, M.Y. Razzaq, A. Lendlein, *Adv. Mater.* **2010**, 22, 3388-3410.
[14] C. Wu, X. Wang, *Phys. Rev. Lett.* **1998**, 80, 4092-4094.
[15] X. Wu, R.H. Pelton, A.E. Hamielec, D.R. Woods, W. McPhee, *Colloid. Polym. Sci.* **1994**, 272, 467-477.
[16] T. Hoare, R. Pelton, *Macromolecules* **2004**, 37, 2544-2550.
[17] L. Hu, M.J. Serpe, *J. Mater. Chem.* **2012**, 22, 8199-8202.
[18] H. Meng, G. Li, *Polymer* **2013**, 54, 2199-2221.
[19] Y. Zhu, J.L. Hu, K.W. Yeung, Y.Q. Liu, H.M. Liem, *J. Appl. Polym. Sci.* **2006**, 100, 4603-4613.
[20] F.L. Ji, J.L. Hu, T.C. Li, Y.W. Wong, *Polymer* **2007**, 48, 5133-5145.
[21] T. Xie, *Polymer* **2011**, 52, 4985-5000.
[22] V. Stroganov, M. Al-Hussein, J.-U. Sommer, A. Janke, S. Zakharchenko, L. Ionov, *Nano Lett.* **2015**, 15, 1786-1790.
[23] X. Li, M.J. Serpe, *Adv. Funct. Mater.* **2014**, 24, 4119-4126.
[24] G. Schwartz, B.C.K. Tee, J. Mei, A.L. Appleton, D.H. Kim, H. Wang, Z. Bao, *Nat. Commun.* **2013**, 4, 1859.
[25] K. Takei, T. Takahashi, J.C. Ho, H. Ko, A.G. Gillies, P.W. Leu, R.S. Fearing, A. Javey, *Nat. Mater.* **2010**, 9, 821-826.
[26] X. Xiao, L. Yuan, J. Zhong, T. Ding, Y. Liu, Z. Cai, Y. Rong, H. Han, J. Zhou, Z.L. Wang, *Adv. Mater.* **2011**, 23, 5440-5444.
[27] T. Yamada, Y. Hayamizu, Y. Yamamoto, Y. Yomogida, A. Izadi-Najafabadi, D.N. Futaba, K. Hata, *Nat. Nanotechnol.* **2011**, 6, 296-301.
[28] D.-H. Kim, J.-H. Ahn, W.M. Choi, H.-S. Kim, T.-H. Kim, J. Song, Y.Y. Huang, Z. Liu, C. Lu, J.A. Rogers, *Science* **2008**, 320, 507-511.
[29] D.-H. Kim, J.A. Rogers, *Adv. Mater.* **2008**, 20, 4887-4892.
[30] T. Sekitani, T. Someya, *Adv. Mater.* **2010**, 22, 2228-2246.
[31] D.-H. Kim, N. Lu, R. Ma, Y.-S. Kim, R.-H. Kim, S. Wang, J. Wu, S.M. Won, H. Tao, A. Islam, K.J. Yu, T.-i. Kim, R. Chowdhury, M. Ying, L. Xu, M. Li, H.-J. Chung, H. Keum, M. McCormick, P. Liu, Y.-W. Zhang, F.G. Omenetto, Y. Huang, T. Coleman, J.A. Rogers, *Science* **2011**, 333, 838-843.

[32] M.L. Hammock, A. Chortos, B.C.K. Tee, J.B.H. Tok, Z. Bao, *Adv. Mater.* **2013**, 25, 5997-6038.
[33] D.-Y. Khang, H. Jiang, Y. Huang, J.A. Rogers, *Science* **2006**, 311, 208-212.
[34] J. Zhong, Q. Zhong, Q. Hu, N. Wu, W. Li, B. Wang, B. Hu, J. Zhou, *Adv. Funct. Mater.* **2015**, 25, 1798-1803.
[35] C. Yan, J. Wang, W. Kang, M. Cui, X. Wang, C.Y. Foo, K.J. Chee, P.S. Lee, *Adv. Mater.* **2014**, 26, 2022-2027.
[36] X. Wang, H. Hu, Y. Shen, X. Zhou, Z. Zheng, *Adv. Mater.* **2011**, 23, 3090-3094.
[37] I.M. Graz, D.P.J. Cotton, S.P. Lacour, *Appl. Phys. Lett.* **2009**, 94, 071902.
[38] A.A. Solovev, S. Sanchez, M. Pumera, Y.F. Mei, O.G. Schmidt, *Adv. Funct. Mater.* **2010**, 20, 2430-2435.
[39] E.J. Smith, Z. Liu, Y.F. Mei, O.G. Schmidt, *Appl. Phys. Lett.* **2009**, 95, 083104.
[40] S. Zakharchenko, N. Puretskiy, G. Stoychev, M. Stamm, L. Ionov, *Soft Matter* **2010**, 6, 2633-2636.
[41] G. Stoychev, N. Puretskiy, L. Ionov, *Soft Matter* **2011**, 7, 3277-3279.
[42] G. Stoychev, S. Zakharchenko, S. Turcaud, J.W.C. Dunlop, L. Ionov, *ACS Nano* **2012**, 6, 3925-3934.
[43] P. Cendula, S. Kiravittaya, I. Mönch, J. Schumann, O.G. Schmidt, *Nano Lett.* **2011**, 11, 236-240.
[44] I.S. Chun, A. Challa, B. Derickson, K.J. Hsia, X. Li, *Nano Lett.* **2010**, 10, 3927-3932.
[45] J. Lu, X. Wang, C. Xiao, *Carbohydr. Polym.* **2008**, 73, 427-437.
[46] S.C. Yeo, A. Eisenberg, *J. Macromol. Sci., B* **1977**, 1977, 13, 441-484
[47] T. Hatakeyama, K. Nakamura, H. Yoshida, H. Hatakeyama, *Thermochim. Acta* **1985**, 88, 223-228.
[48] K. Nakamura, T. Hatakeyama, H. Hatakeyama, *Polym. J.* **1991**, 23, 253-258.
[49] N. Lambricht, T. Pardoen, S. Yunus, *Acta Mater.* **2013**, 61, 540-547.
[50] P. Gorrn, W. Cao, S. Wagner, *Soft Matter* **2011**, 7, 7177-7180.
[51] C.D. Sorrell, M.J. Serpe, *Adv. Mater.* **2011**, 23, 4088-4092.

Acknowledgments

MJS acknowledges funding from the University of Alberta (the Department of Chemistry and the Faculty of Science), the Natural Sciences and Engineering Research Council of Canada (NSERC), the Canada Foundation for Innovation (CFI), the Alberta Advanced Education & Technology Small Equipment Grants Program (AET/SEGP), Grand Challenges Canada and IC-IMPACTS. XL acknowledges Alberta Innovates Technology Futures (AITF) for graduate student scholarships.

Figures

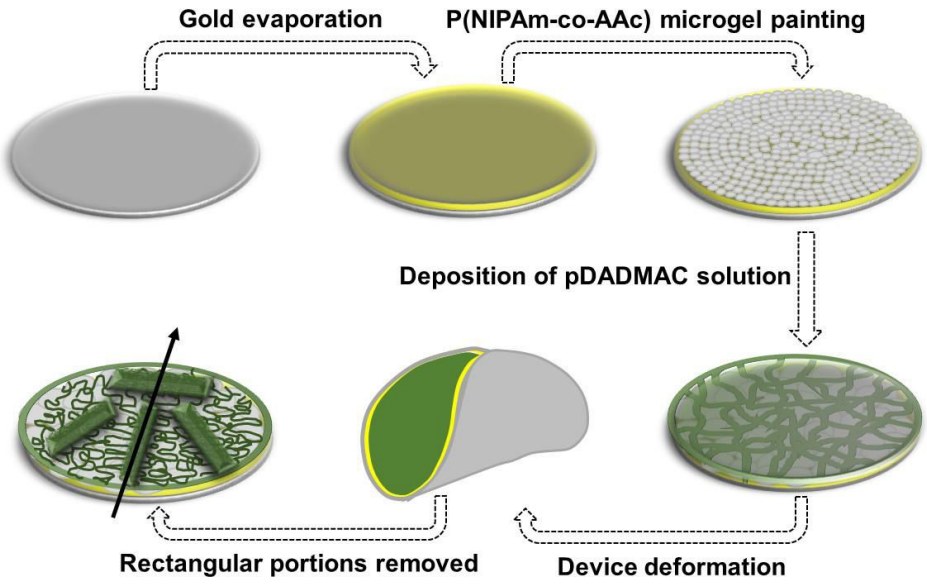

Figure 1. Bilayer fabrication process showing the bending behavior, and the bending axis (black arrow). Rectangular pieces can be cut from this bilayer at various orientations relative to the bending axis.

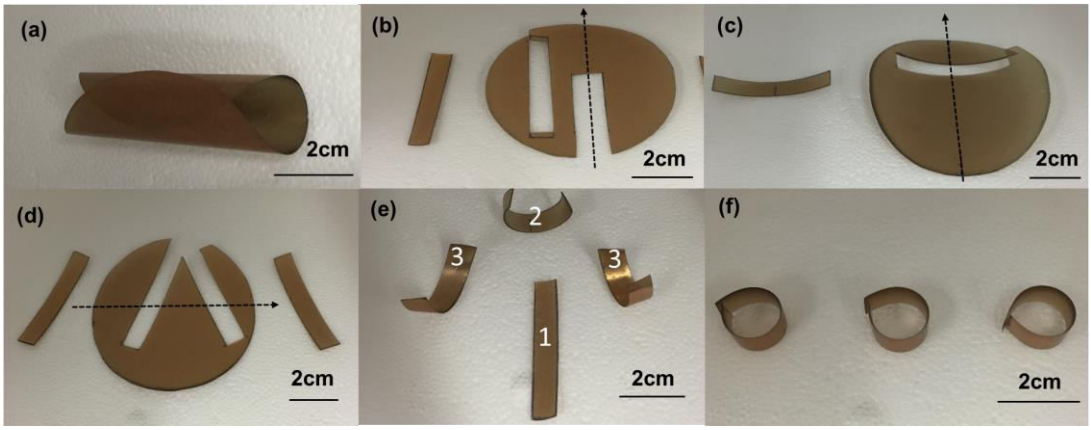

Figure 2. (a) A bent circular device; (b, c, d) Rectangular pieces cut from three different opened circular devices — the arrows indicate the bending axis on each device; (e) Bent rectangular devices cut from prebent circular bilayers — e1 is from b, e2 is from c, e3 are

from d; (f) Bent rectangular devices with the same dimensions of the devices in (e), but these devices were cut from pieces that were not prebent.

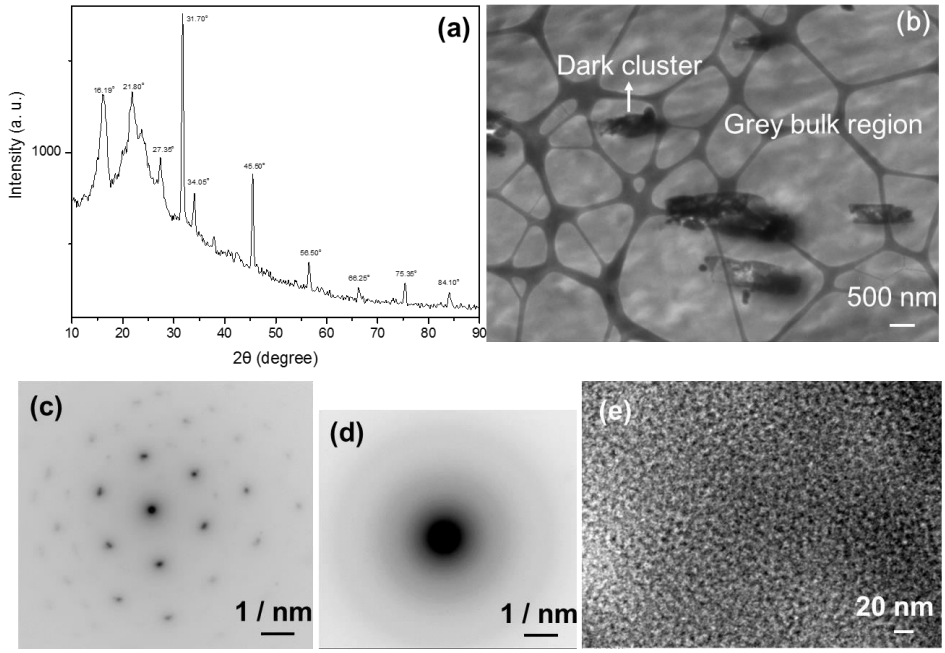

Figure 3. (a) X-ray diffraction pattern of pDADMAC layer; (b) TEM image of pDADAMAC layer — dark "web-like" features are from the TEM grid; (c) Electron diffraction pattern of cluster of the microtomed thin pDADMAC film; (d) Electron diffraction pattern of polymer portion of the film; (e) TEM image of the polymer portion of the film.

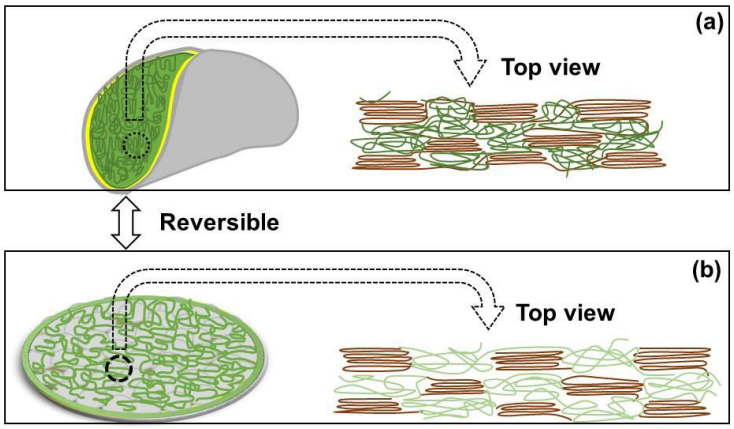

Figure 4. (Left) Schematic of the bent and unbent circular devices and (right) the corresponding proposed pDADMAC phases. Top views are the x-y of each circled region.

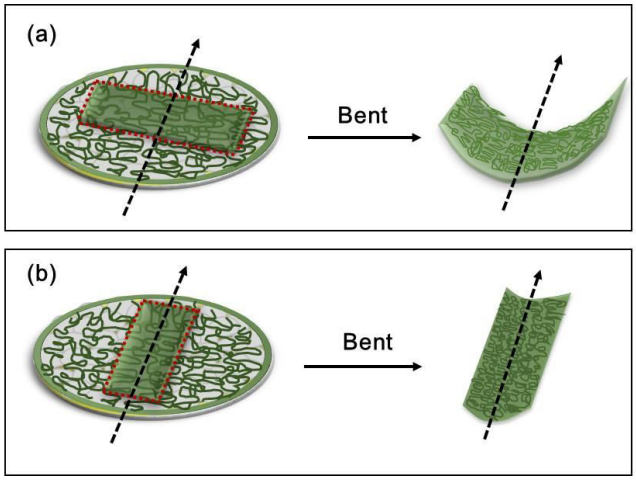

Figure 5. Schematic of the bent rectangular portions cut from the shaded regions of the (left) circular devices. (a) Rectangular device's long axis cut perpendicular to the bending axis; (b) Rectangular device's long axis cut parallel to the bending axis.

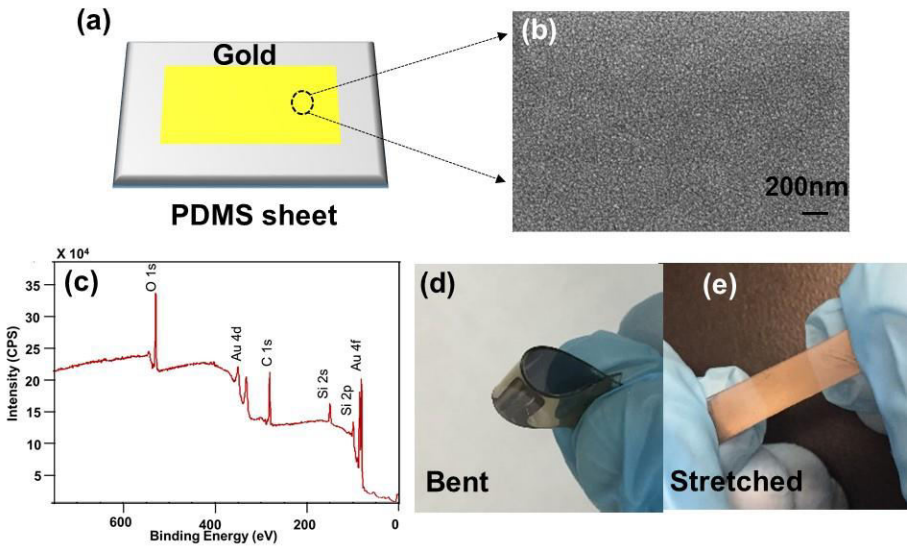

Figure 6. (a) Schematic depiction of the strain sensor; (b) FESEM images of the surface of the strain sensor after fabrication; (c) XPS of the gold coated PDMS substrate; (d,e) bent and stretched strain sensors.

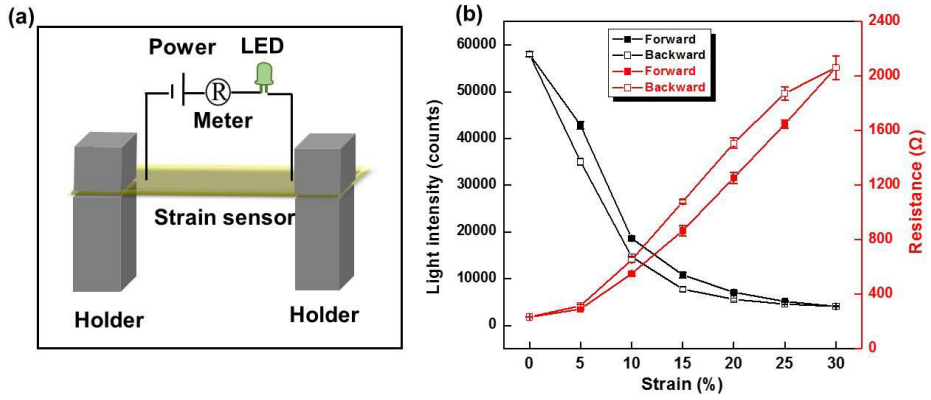

Figure 7. (a) Schematic depiction of the setup used to monitor resistance (and LED intensity) as a function of strain. (b) LED light intensity (left axis) resistance (right axis) and as a function of strain. In all cases, each data point is the average signal obtained from a single device measured three times, while the error bars is the standard deviation.

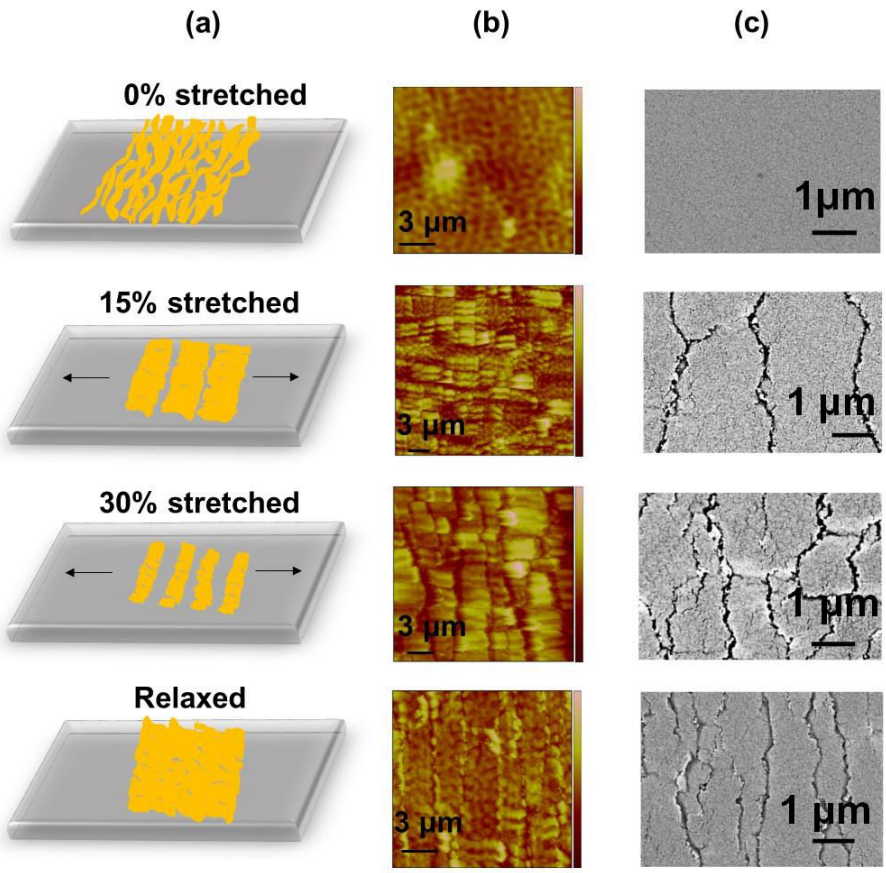

Figure 8. (a) Schematic depiction of the Au morphology as a function of strain and the corresponding; (b) AFM; and (c) FESEM images at the indicated strains.

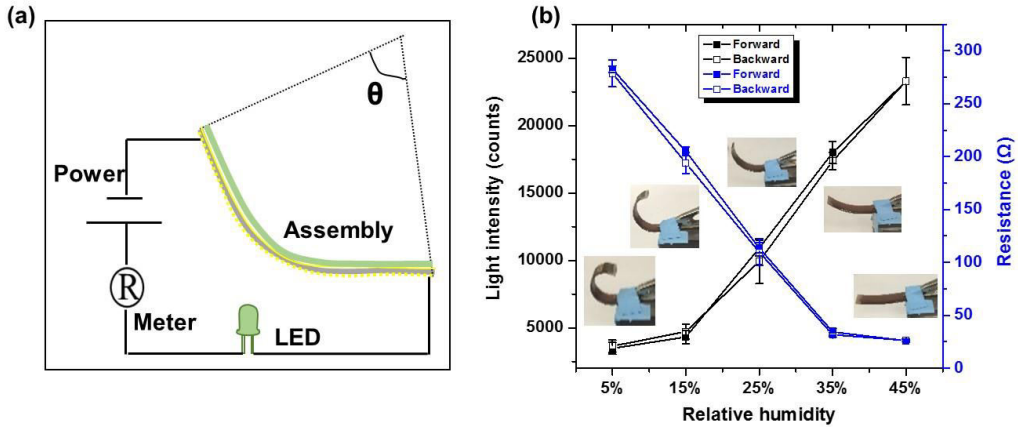

Figure 9. (a) Schematic depiction of the experimental setup used to measure resistance and LED light intensity as a function of device bending; (b) Light intensity (left axis) and resistance (right axis) changes induced by the bending of the bilayers coupled to the strain sensors. In all cases, each data point is the average signal obtained from a single device measured three times, while the error bars is the standard deviation.